Eur. Phys. J. D **14**, 309–316 (2001)

THE EUROPEAN PHYSICAL JOURNAL D

EDP Sciences

Tight-binding study of structural and electronic properties of silver clusters

J. Zhao[1,2,a], Y. Luo[3], and G. Wang[3]

[1] Department of Physics and Astronomy, University of North Carolina at Chapel Hill, Chapel Hill, NC 27599, USA
[2] International Centre for Theoretical Physics, P.O. Box 586, Trieste 34100, Italy
[3] National Laboratory of Solid State Microstructures, Nanjing University, Nanjing 210093, P.R. China

Received 7 August 2000

Abstract. Tight-binding model is developed to study the structural and electronic properties of silver clusters. The ground state structures of Ag clusters up to 21 atoms are optimized by molecular dynamics-based genetic algorithm. The results on small Ag_n clusters ($n = 3$–9) are comparable to *ab initio* calculations. The size dependence of electronic properties such as density of states, s–d band separation, HOMO-LUMO gap, and ionization potentials are discussed. Magic number behavior at Ag_2, Ag_8, Ag_{14}, Ag_{18}, Ag_{20} is obtained, in agreement with the prediction of electronic ellipsoid shell model. We suggest that both the electronic and geometrical effect play significant role in the coinage metal clusters.

PACS. 36.40.Cg Electronic and magnetic properties of clusters – 36.40.Mr Spectroscopy and geometrical structure of clusters – 71.24.+q Electronic structure of clusters and nanoparticles

1 Introduction

The structural and electronic properties of metal clusters have been a field of intensive research both theoretically and experimentally [1–5]. The basic theoretical concept in the electronic structure of metal clusters is the shell model based on jellium sphere (or ellipsoid) approximation [2,3,5]. It has successfully interpreted the magic number effect in alkali-metal clusters Na_n and K_n ($n = 2, 8, 20, 40, ...$). As compared with alkali-metal clusters, the application of electronic shell model to coinage-metal clusters (Cu_n, Ag_n, Au_n) is more questionable because of the inner d electrons. Among noble metal clusters, Ag_n is expected to exhibit the largest similarity to the alkali metal clusters as the $4d$ orbitals in Ag atom are low-lying and act almost like innershell core orbitals.

Experimental studies on silver clusters include mass-spectra [6], ionization potentials (IPs) [7,8], photoelectron spectra [9–11], electron spin resonance (ESR) [12,13], optical resonance absorption [14–16], electron diffraction [17], photofragmentation [18], dissociation energies [19], etc. In general, most of the cluster properties resemble the predictions of shell model within one s electron picture. But there are still some experimental evidences on Ag_n that are different with those of alkali-metal clusters and cannot be understood by the s electron shell model. For instance, the Mie resonance peak of silver clusters demonstrates blue shift with decreasing cluster radius [14], while red shift of Mie resonance frequency is found for alkali-metal clusters [4]. A direct comparison of photoelectron spectra between Ag_n and Na_n show significant difference caused by the d orbitals [10]. Therefore, it is important to clarify the contribution of $4d$ electrons and s–d interaction in the silver clusters and the geometrical effect on the electronic properties of the clusters.

Besides shell model, the metal clusters can be investigated by accurate quantum chemical methods [1]. However, such *ab initio* calculations on coinage metal clusters are quite time consuming and limited in small size [20–24]. Among those works, the most detailed and comprehensive study of small neutral silver clusters (Ag_2 to Ag_9) has been performed *via* configuration interaction (CI) method with relativistic effective core potential (RECP) [22]. However, all these studies are carried out for limited number of structural candidates with symmetry constrain. An unbiased structural minimization incorporated with electronic structure calculations will be much more informative for understanding the interplay between geometrical and electronic effect as well as the validity of electronic shell model.

Up to now, the most practical and affordable first principles method in dynamic searching of cluster equilibrium geometries is provided by Car-Parrinello (CP) method with simulated annealing (SA) [25,26]. However, such *ab initio* simulations are also limited in small size (about $n \leq 10$–20) in a truly global optimization, since the computational expense increases rapidly with cluster size. Among coinage metal clusters, the CP method has been employed to study small Cu_n clusters ($n = 2$–10) [27] and Ag_n ($n = 4$, 5, 6) [28]. As an alternative approach to CP

[a] e-mail: zhaoj@physics.unc.edu

Table 1. Parameters of TB model for silver used in this work.

ϵ_s	ϵ_p	$\epsilon_{d,xy}$	ϵ_{d,x^2-y^2}
−6.452 eV	−0.447 eV	−14.213 eV	−14.247 eV

$V_{ss\sigma}$	$V_{sp\sigma}$	$V_{pp\sigma}$	$V_{pp\pi}$	$V_{sd\sigma}$
−0.895 eV	1.331 eV	2.143 eV	0.088 eV	−0.423 eV

$V_{pd\sigma}$	$V_{pd\pi}$	$V_{dd\sigma}$	$V_{dd\pi}$	$V_{dd\delta}$
−0.531 eV	0.207 eV	−0.429 eV	0.239 eV	−0.046 eV

d_0	α	χ_0	a	b	R_c	Δ
2.89 Å	0.692 Å^{-1}	0.58 eV	−0.16 eV	0.59 eV	3.5 Å	0.1 Å

method, tight-binding molecular dynamics (TBMD) has been introduced in atomistic simulation for larger systems [29]. As compared to *ab initio* methods, the parameterized tight-binding (TB) Hamiltonian dramatically reduces the computational cost. It is still more reliable than empirical MD simulation because the atomic motion is directly coupled with electronic structure calculation at each step. For transition-metal clusters, Menon and co-workers have proposed a minimal parameter tight-binding scheme and used it to study nickel and iron clusters [30,31]. In this work, we develop a TB model for silver. Genetic algorithm (GA) [32–35] is used to search the global minimal structure of Ag_n clusters up to 21 atoms. The size dependence of relative stabilities, density of states (DOS), electronic gaps, and ionization potentials (IPs) of the clusters are calculated and compared with available experimental results. The magic number effect of electronic shell and the interplay between geometrical and electronic structure in silver clusters are discussed.

2 Theoretical method

In the minimal parameter tight-binding scheme proposed by Menon *et al.* [30], the total binding energy E_b of transition-metal atoms is written as a sum:

$$E_b = E_{el} + E_{rep} + E_{bond}. \quad (1)$$

E_{el} is the electronic band structure energy defined as the sum of one-electron energies for the occupied states

$$E_{el} = \sum_k^{occ} \epsilon_k \quad (2)$$

where energy eigenvalues ϵ_k can be obtained by solving orthogonal $9n \times 9n$ TB Hamiltonian including $4d$, $5s$ and $5p$ electrons. The repulsive energy E_{rep} is described by a pair potential function $\chi(r)$ of exponential form:

$$E_{rep} = \sum_i \sum_{j>i} \chi(r_{ij}) = \sum_i \sum_{j>i} \chi_0 e^{-4\alpha(r_{ij}-d_0)} \quad (3)$$

where r_{ij} is the separation between atom i and j, $d_0 = 2.89$ Å is the bond length for the fcc bulk silver [36], α is taken to be one-half of $1/d_0$ according to reference [30].

In order to reproduce the cohesive energies of small clusters through bulk TB hopping parameters, it is still necessary to introduce a bond-counting term E_{bond}:

$$E_{bond} = -N[a(n_b/N) + b]. \quad (4)$$

Here the number of bonds n_b are evaluated by summing over all bonds according to cutoff distance R_c and bond length d_i

$$n_b = \sum_i \left[\exp\left(\frac{d_i - R_c}{\Delta}\right) + 1\right]^{-1}. \quad (5)$$

As in reference [30], only the first two terms E_{el} and E_{rep} in equation (1) are used to compute the interatomic forces in TBMD simulation, while the E_{bond} term is added after the relaxation has been achieved as an approximation. For metal clusters, such correction term is significant in distinguishing various isomers at a given cluster size [30].

The $9n \times 9n$ TB Hamiltonian matrix is constructed with Slater-Koster scheme, while the distance scaling of hopping integrals $V_{\lambda\lambda'\mu}$ is taken as the Harrison's universal form [37]:

$$V_{\lambda\lambda'\mu}(d) = V_{\lambda\lambda'\mu}(d_0)\left(\frac{d_0}{d}\right)^{\tau+2}. \quad (6)$$

The parameter $\tau = 0$ for s–s, s–p, p–p interactions, $\tau = 3/2$ for s–d and p–d interaction, $\tau = 3$ for d–d interaction.

In present, we have adopted the Slater-Koster hopping integrals $V_{\lambda\lambda'\mu}(d_0)$ and the on-site orbital energy from the values fitted to first principle APW band structure calculation of bulk silver [38]. Furthermore, to transfer the on-site orbital energies levels from bulk calculation to atomic limit, a constant energy shift $\Delta\epsilon = -15.88$ eV is applied on the on-site energies from reference [38]. Such shift in on-site levels make the theoretical ionization potential of Ag_n clusters quantitatively comparable to experimental values. The repulsive potential parameter χ_0 is fitted for experimental bond length 2.48 Å of silver dimer [39]. The bond-counting terms a, b are chosen to reproduce the *ab initio* binding energy for small clusters Ag_3, Ag_4, Ag_5 [20,22,23]. All the parameters used in our calculation are given in Table 1. These empirical parameters can describe both bulk phase and dimer of silver with an acceptable accuracy. The cohesive energy 2.75 eV, equilibrium interatomic distance 2.88 Å of fcc silver solid from TB model

are close to the experimental value 2.95 eV and 2.89 Å respectively [36]. The vibrational frequency and binding energy calculated for silver dimer at equilibrium distance is 125.5 cm^{-1} and 1.25 eV, in reasonable agreement with the value of 192.4 cm^{-1} and 1.66 eV from experiments [39]. In addition, a better agreement between the experimental and the TBMD results for the vibrating frequencies can be obtained if the parameter a is fitted in such a way like reference [46] so as the TBMD results can reproduce the experimental vibrational frequency of the Ag_2 dimer. It is worthy to note that that current tight-binding model might cause certain charge transfer between the atoms which are not geometrically equivalent. Typically, a Hubbard-like term should be included in the on-site energy of tight-binding Hamiltonian to prevent the possible unphysical charge transfer. However, in this work, we have not included this correction term as an approximation.

The lowest energy structures of clusters is determined by a genetic algorithm [32–35]. The essential idea of its strategy is to mimic the Darwinian biological evolution process in which only the fittest candidate can survive. Some pioneering works have demonstrated the impressive efficiency of GA in searching the global minima of clusters as compared to standard simulated annealing [32]. At beginning, we generate a number N_p of initial configurations by random ($N_p = 4$–16, depending on cluster size). Any two candidates in this population can be chosen as parents to generate a child cluster through the mating process. In the end of mating procedure, mutation operation is allowed to apply on the configuration of child cluster with 30% possibility. The child cluster from each generation can be relaxed by tight-binding molecular dynamics minimization. Thus the locally minimized child is selected to replace its parent in the population if it has different geometry but lower binding energy. Typically, 200 GA iterations is sufficient to ensure a truly global search up to $n = 21$.

3 Structures and stabilities of sliver clusters

3.1 Structures of small Ag_n with $n \leq 9$

In this work, we have explored the global minimal structures of Ag_n clusters up to 21 atoms. The ground state structures are shown in Figure 1 ($4 \leq n \leq 9$) and Figure 2 ($10 \leq n \leq 21$). In Table 2, the structural parameters, binding energies and ionization potentials of the small Ag_n clusters ($n = 3$–9) of ground state and some stable isomers are compared with accurate quantum chemistry calculations [20–23]. Most of the lowest energy structures found for the clusters are consistent with CI calculations [22] and the other *ab initio* studies [20–22]. The calculated cluster properties of ground state and stable isomers are also comparable to the *ab initio* results. As shown in Table 1, the TB bond lengths are typically within 0.05−0.15 Å according to the *ab initio* values. The average deviation of binding energy per atom and ionization potentials from this work to *ab initio* calculations [22] is about 0.13 eV and 0.30 eV respectively.

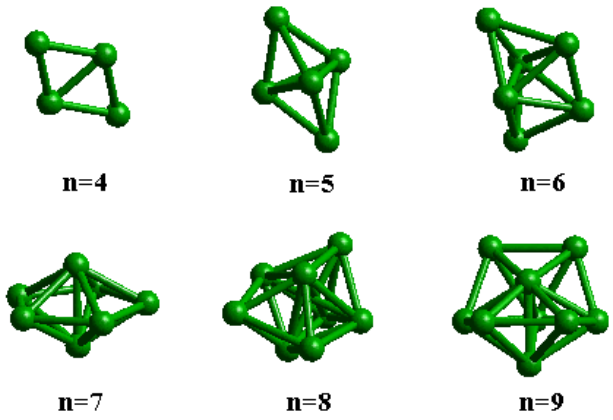

Fig. 1. Lowest-energy structures for Ag_n ($n = 4$–9) clusters.

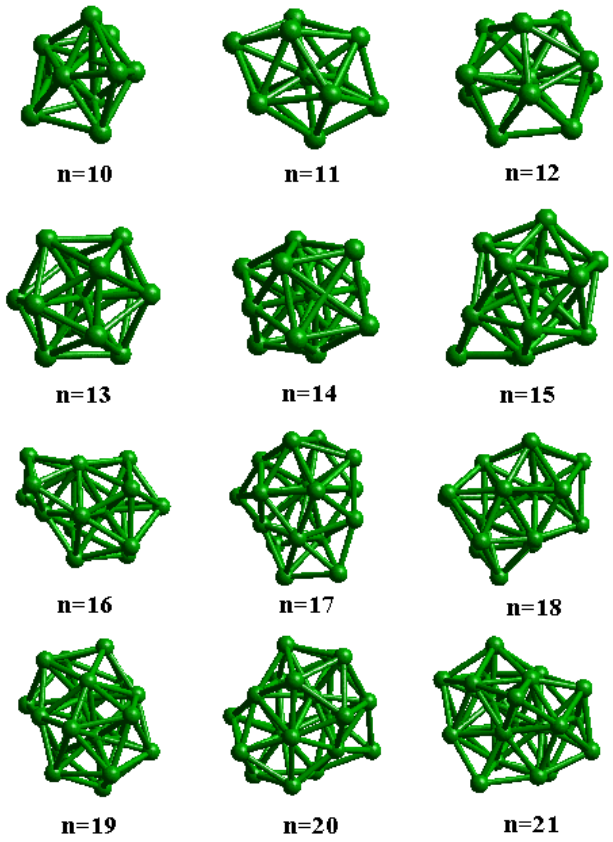

Fig. 2. Lowest-energy structures for Ag_n ($n = 10$–21) clusters. See text for description of structures.

For silver trimer, we found the isosceles triangle structure with C_{2v} symmetry, which is supported by ESR experiments on Ag_3 [12]. In the case of Ag_4, planar rhombus is lower in energy than a relaxed tetrahedron by $\Delta E = 0.31$ eV. As shown in Table 2, both of these structures for Ag_3 and Ag_4 agree well with *ab initio* results [20–23, 28].

The lowest energy structure found for Ag_5 is a compressed trigonal bipyramid, which has lower energy ($\Delta E = 0.17$ eV) than a planar capped rhombus. In previous studies, the planar structure has been obtained as

Table 2. Bond length, bond angle, average binding energies E_b/n, and vertical ionization potentials (IP) of small Ag_n ($n = 3$–9) clusters obtained from TB calculation compare with *ab initio* calculations [20–23]. The definition of structural parameters r, α, h, etc. for smaller Ag_{3-5} clusters is chosen according to reference [22]; the bonds for Ag_{6-9} are defined by their lengths in reference [22] in a declining sequence. *a* denotes our present tight-binding calculation. *b* to *e* are previous *ab initio* calculations based on relativistic effective core potential configuration (RECP): *b*-modified coupled pair function (MCPF) [20]; *c*-multireference singles plus doubles configuration (MRSDCI) [21]; *d*-configuration interaction (CI) [22]; *e*-relativistic effective core potential density functional theory (RECP-DFT) [23].

Ag_3, obtuse triangle (C_{2v})

	r (Å)	α (deg)	E_b/n (eV)	IP (eV)
a	2.659	66.8	0.82	5.65
b	2.709	69.2	0.80	5.59
c	2.720	63.7	0.90	5.90
d	2.678	69.1	0.86	5.74
e	2.627	70.4	0.84	–

Ag_4, rhombus (D_{2h})

	r (Å)	α (deg)	E_b/n (eV)	IP (eV)
a	2.731	56.6	1.21	6.86
b	2.862	57.6	1.11	6.54
c	2.870	55.5	1.83	6.40
d	2.800	56.4	1.20	6.60
e	2.740	57.2	1.11	–

Ag_5, deformed trigonal bipyramid (C_{2v})

	r (Å)	α (deg)	$h/2$ (Å)	E_b/n(eV)	IP (eV)
a	2.749	67.5	2.34	1.38	5.88
b	2.858	65.8	2.39	1.16	–
d	2.709	67.8	2.33	1.28	5.95

Ag_5, planar capped rhombus (C_{2v})

	r_1 (Å)	r_2 (Å)	r_3 (Å)	r_4 (Å)	E_b/n(eV)	IP (eV)
a	2.851	2.736	2.740	2.668	1.32	6.20
b	2.842	2.842	2.842	2.842	1.22	6.18
d	2.812	2.801	2.760	2.759	1.28	6.20

Ag_6, bicapped tetrahedron (C_{2v})

	r_1 (Å)	r_2 (Å)	r_3 (Å)	r_4 (Å)	r_5 (Å)	E_b/n(eV)	IP(eV)
a	2.931	2.875	2.766	2.653	2.661	1.65	6.71
d	2.976	2.859	2.783	2.751	2.672	1.49	6.23

Ag_6, pentagonal pyramid (C_{5v})

	r_1 (Å)	r_2 (Å)	E_b/n(eV)	IP (eV)
a	2.984	2.539	1.65	7.92
d	2.828	2.740	1.50	7.00

Ag_7, pentagonal bipyramid (D_{5h})

	r_1 (Å)	r_2 (Å)	E_b/n(eV)	IP (eV)
a	2.879	2.858	1.87	5.95
d	2.815	2.806	1.71	5.91

Ag_8, bicapped octahedron (D_{2d})

	r_1 (Å)	r_2 (Å)	r_3 (Å)	r_4 (Å)	E_b/n(eV)	IP(eV)
a	3.140	2.812	2.941	2.661	2.03	7.10
d	2.973	2.812	2.804	2.735	1.80	6.80

Ag_9, bicapped pentagonal bipyramid (C_{2v})

	r_1 (Å)	r_2 (Å)	r_3 (Å)	r_4 (Å)	r_5 (Å)
a	2.989	2.936	2.993	2.888	2.856
d	2.934	2.887	2.881	2.836	2.786

	r_6 (Å)	r_7 (Å)	E_b/n(eV)	IP(eV)
a	2.849	2.745	2.09	5.74
d	2.766	2.752	1.77	5.10

ground state [20,22,23,28] but the energy difference between these two isomers is small ($\Delta E = 0.31$ eV in Ref. [20] and $\Delta E = 0.003$ eV in Ref. [22]). It is noted that different experimental ESR spectra of Ag_5 have been interpreted by both deformed trigonal bipyramid [12] and planar structure [13].

Two isoenergitic structures, a bicapped tetrahedron and a pentagonal pyramid are found for Ag_6, with $\Delta E = 0.05$ eV. The bicapped tetrahedron is more stable. In reference [22], these two structures are also found to be very close in energy ($\Delta E = 0.06$ eV) but the pentagonal pyramid is ground state.

The pentagonal bipyramid is obtained as lowest energy structure for Ag_7. The tricapped tetrahedron is a locally stable isomer with $\Delta E = 0.48$ eV. The pentagonal bipyramid is also obtained as ground state in previous *ab initio* calculations [22]. Moreover, the ΔE for the same tricapped tetrahedron isomer is 0.41 eV in reference [22]. The present ground state structure is also supported by a recent relativistic calculation on spin distribution and magnetic hyperfine tensor [40].

For silver octamer, a bicapped octahedron is our ground state structure, which is also found for Cu_8 [27]. The tetracapped tetrahedron that was predicted as metastable isomer in reference [22] is unstable upon relaxation in our calculations. Square antiprism (D_{4d}) is found as a local stable isomer with $\Delta E = 0.99$ eV.

For Ag_9, the ground state structure is a bicapped pentagonal bipyramid. Its energy is lower than that of the tricapped trigonal prism (C_{3v}) by 0.59 eV and than that of capped square antiprism (C_{2v}) by 1.01 eV. In reference [22], bicapped pentagonal bipyramid is also found as ground state and the energy difference ΔE for the two structural isomers is 0.73 eV and 0.22 eV respectively.

From above discussions, we find the overall agreement between TB model and *ab initio* calculations is reasonable, particularly considering the simplicity in the tight-binding scheme. Therefore, we shall use this model to study larger clusters with $n \geq 10$ in the next part, for which the global minimization with *ab initio* molecular dynamics is much more expensive.

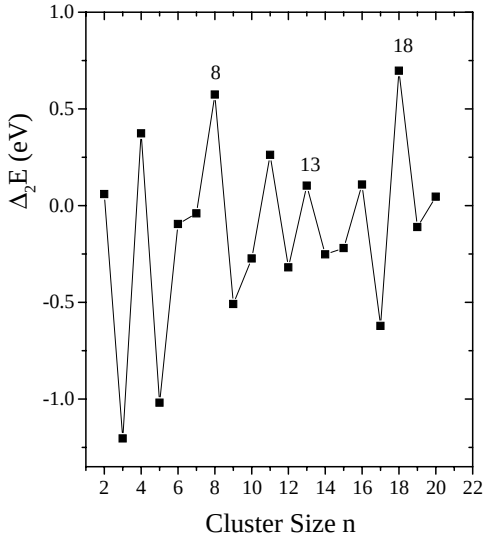

Fig. 3. Second differences of binding energies $\Delta E(n) = [E_b(Ag_{n-1}) + E_b(Ag_{n+1})] - 2E_b(Ag_n)$ as a function of cluster size n for $n = 2$–21. Both electronic shell effect at $n = 8$, 18 and geometrical shell effect at Ag_{13} can be identified. See text for details.

3.2 Structures of Ag_n with $10 \leq n \leq 21$

The lowest energy structure of Ag_n ($n = 10$–21) obtained from GA-TBMD simulation is shown in Figure 2. The most stable structure of Ag_{10} is a deformed bicapped square antiprism (D_{4d}), which is similar to that found for Cu_{10} [27]. Starting from Ag_{11}, the ground state structures of Ag_n clusters are based on icosahedral packing, except for Ag_{14}. Many other capped polyhedral structures are obtained as local isomers for Ag_n with $n = 10$–21 but it is not necessary to describe them here. As shown in Figure 2, the structures of Ag_{11}, Ag_{12} are the uncompleted icosahedron with lack of one or two atoms. An Jahn-Teller distorted icosahedron is then formed at Ag_{13}.

Following the icosahedral growth sequence, the lowest energy structures of Ag_{15}, Ag_{16}, Ag_{17} is the icosahedron capped with 2, 3, 4 atoms respectively. The capped single icosahedron transits into an truncated double icosahedron at Ag_{18} and a complete double icosahedron at the Ag_{19}. Base on the double icosahedron structure, the structures of Ag_{20} and Ag_{21} is formed by one and two atoms capped on that of Ag_{19}. However, an exception occur at Ag_{14}, for which we found fcc-like packing with 4–1–4–1–4 layered structure. It is more stable than a capped icosahedron structure by 0.03 eV.

3.3 Size dependence of relative stabilities

The second differences of cluster binding energies defined by $\Delta_2 E(n) = E_b(n+1) + E_b(n-1) - 2E_b(n)$ is calculated and plotted in Figure 3. In cluster physics, the $\Delta_2 E(n)$ is a sensitive quantity that reflect the stability of clusters and can be directly compared to the experimental relative abundance. Three major characteristics can be found in Figure 3:

(i) even-odd alternation of $\Delta_2 E(n)$ with $n = 2$–6, 15–21;
(ii) particular high peak at Ag_8, Ag_{18};
(iii) other maxima at odd size like Ag_{13} and Ag_{11}.

The first effect can be related to the even-odd oscillation of HOMO energy and HOMO-LUMO gap in silver clusters, which is due to electron pairing effect. The particular stable clusters such as Ag_8, Ag_{18} corresponds to the magic number in electronic shell model. However, the even-odd oscillation in $\Delta_2 E(n)$ from Ag_{10} to Ag_{14} and the maximum at magic size Ag_{20} have not been observed in our calculation. In stead, some odd-sized cluster as Ag_{11}, Ag_{13} become maxima in Figure 3. These phenomena can be attributed to the geometrical effect. The closing of geometrical shell of icosahedron at Ag_{13} will enhance the stability of such clusters and reduce the relative stability of their neighboring clusters.

The simultaneous appearance of those three features in the $\Delta_2 E(n)$ demonstrates that the structure and stability of a silver cluster is determined by both electronic structure and atomic configuration. Either electronic or geometrical effect is enhanced if the corresponding shell structure is completed. This argument is supported by a experimental probe of geometrical and electronic structure of copper clusters [41]. They found both jellium-like electronic behavior and icosahedral geometrical structure in copper clusters. In a experimental studies of mass spectra of ionized silver clusters [6], dramatic even-odd oscillation as well as substantial discontinuities at electronic magic number 8, 20 ($n = 9$, 21 for cationic clusters) are found. The discrepancy between present theoretical result and experiment may be partially attributed to the effect of ionization on the cluster stability. Since the experimental mass spectra distribution is recorded for ionized clusters Ag_n^+, it is possible that the charging on the cluster can significantly alter the geometrical and electronic structure of the cluster [1,22].

4 Electronic properties vs. cluster size

4.1 Size evolution of electronic band

We investigated the cluster electronic properties by looking up the electronic density of states (DOS). In Figure 4, we present the total *spd* electronic DOS for Ag_2, Ag_8, Ag_{13} along with bulk DOS of fcc crystal silver from TB calculation in reciprocal space. The electro DOS are obtained from a 0.02 eV Gaussian broadening of cluster electronic levels. Typically, the total DOS is composed by the relatively compact d states and the more expanded *sp* states. In the smallest clusters like Ag_2, the d and *sp* bands are clearly separated. The *sp* states shows discrete peaks originated from symmetrical splitting of atomic orbital levels, while the d band is low-lying and considerably narrower than the bulk d band. In contrast to even-odd behavior and shell occupation of s electrons, the evolution of d states from smallest clusters towards bulk solid is a monotonic broaden of band width. As the cluster size increases,

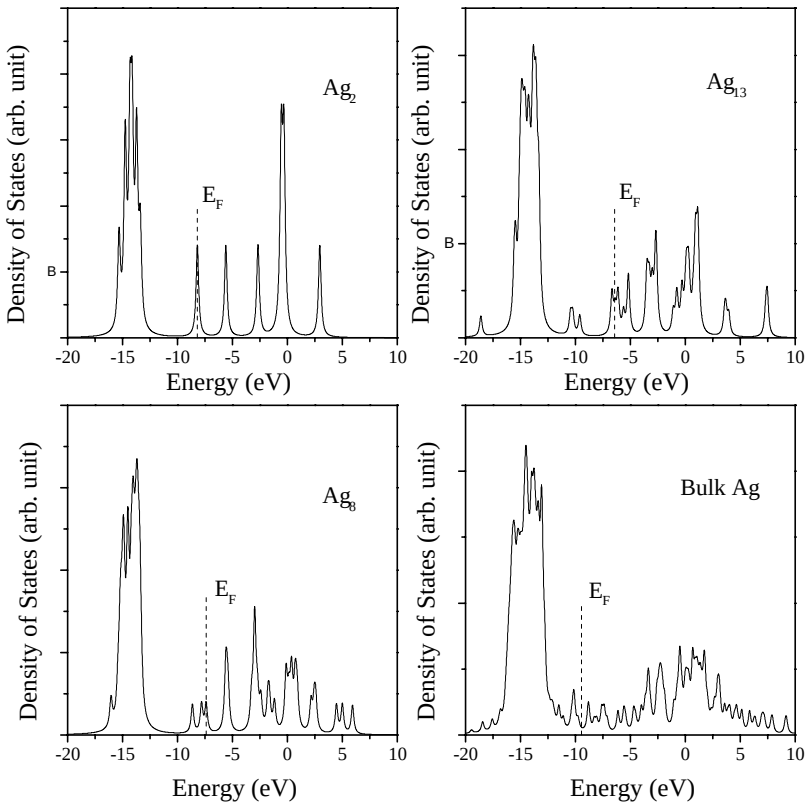

Fig. 4. Density of states (DOS) of Ag_n ($n = 2$, 8, 13) clusters *vs.* cluster as well as bulk DOS in fcc crystalline (with Gaussian broaden of 0.02 eV).

both d and sp levels gradually broaden, shift, overlap with each other, and finally come into being bulk electronic band. The DOS of Ag_8 still has molecular-like feature such as the discrete sp peaks. But these electronic spectra peaks tend to overlap and form continuous band. In Ag_{13}, the sp states have developed into several subbands and the d band has overlapped with sp states. Although the DOS of Ag_{13} is roughly similar to the bulk limit, the width of d band is still considerably narrower than the bulk d band width and the fine structure of sp electronic spectra is different from bulk sp band. This fact suggests that the bulk-like behavior emerge at around Ag_{13}. We have also studied the electronic states of Ag_{55} with icosahedral and cuboctahedral structures by using present tight-binding scheme with local minimization. The DOS for both of them are very close to bulk band. In a previous experimental study of photoelectron spectra of silver clusters up to 60 atoms [10], the ultraviolet photoelectron spectroscopy (UPS) of smallest Ag_n, *i.e.*, $2 \leq n \leq 10$ is different from bulk UPS and changes sensitively on cluster size. The size dependent variation of UPS for Ag_n with $n < 10$ becomes more gradual and the UPS of Ag_{60} is already very similar to that of solid silver.

To further clarify the size evolution of the overlap of d and sp bands in the small silver clusters, we have examined the energy separation Δ_{sd} between the highest molecular orbitals belong to d states and lowest molecular orbitals from s states. The calculated Δ_{sd} decrease rapidly from 5.20 eV for Ag_2, to 1.69 eV for Ag_5 and then to 0.10 eV for Ag_8. Finally, the d and sp band merge in Ag_n clusters with $n \geq 9$. The overlap between s and d band can be related to the icosahedral growth sequence starting from Ag_{11} and weakening of the even-odd oscillation in HOMO-LUMO gaps and IPs with $n > 10$. However, the overlap between sp and d states is small and the cluster HOMO is located in the s-like electronic states. The electronic behaviors related to Fermi energy such as HOMO-LUMO gap, ionization potentials are probably still dominated by s orbitals.

4.2 HOMO-LUMO gaps

An important electronic property of a cluster is the gap between highest occupied molecular orbital (HOMO) and lowest unoccupied molecular orbital (LUMO). In the case of magic cluster, the closure of electronic shell shall manifest itself in particularly large HOMO-LUMO gap. This effect was demonstrated experimentally for small even-sized silver and copper clusters [9] and theoretically for copper clusters [42,43]. The theoretical HOMO-LUMO gap of Ag_n ($n = 2$–21) along with experimental gap of small clusters Ag_n ($n = 2$, 4, 6, 8, 10) [9] are shown in Figure 5. Even-odd oscillation up to Ag_{16} as well as the particularly large HOMO-LUMO gap at Ag_2, Ag_8, and Ag_{18} are obtained. As compared to the experimental results for small Ag_n with even size, the present TB calculation has systematically overestimated the HOMO-LUMO electronic gap by about 0.5 eV. But the size dependent variation of experimental gaps and magic effect in HOMO-LUMO gaps at $n = 2$, 8 are qualitatively reproduced. The even-odd alternation for $n \geq 16$ and magic effect of Ag_{20} have

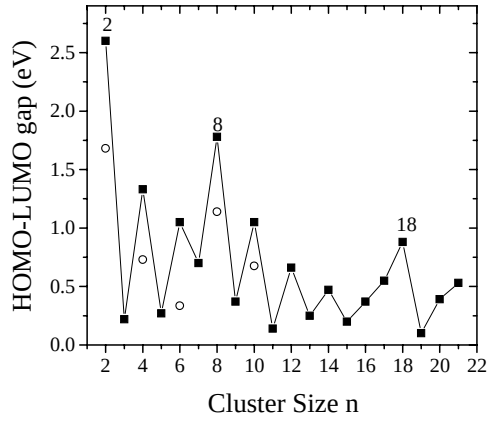

Fig. 5. HOMO-LUMO gap *vs.* cluster size n. The theoretical values are labeled by solid square connected with solid line and the experimental values in reference [9] are labeled by open circles. Electronic shell effect for $n = 2$, 8, 18 can be clearly identified.

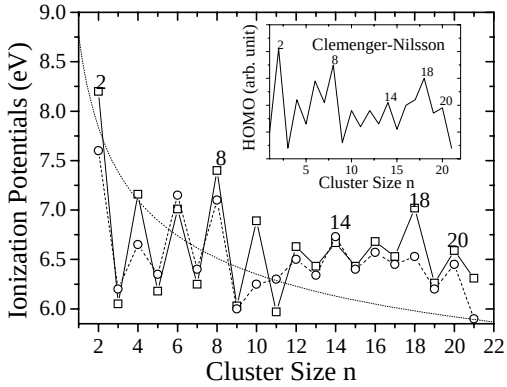

Fig. 6. Vertical ionization potentials (IPs) *vs.* cluster size n. The measured IP values reported in reference [7] are labeled by open circles connected with dashed line, the theoretical values from TB calculation are labeled by open squares connected with solid line. Electronic shell closing exhibit as pronounced raises of IP at $n = 2$, 8, 14, 18, 20. See text for details.

not been obtained in our calculation. We suggest these are probably due to the geometrical effect, since the HOMO-LUMO gap of cluster depends sensitively on cluster structure [42]. In a previous study of HOMO-LUMO gaps of copper clusters [42], the maxim gap at Cu_8 and Cu_{20} is found but the even-odd alternation of electronic gap and magic effect for Cu_{18} have not been obtained.

4.3 Ionization potentials

The vertical ionization potentials (IPs) of clusters are evaluated from the HOMO energy of neutral clusters according to Koopman's theorem. In Figure 6, the calculated IPs of Ag_n up to $n = 21$ is compared with the IP values measured by Jackschath [7] and the prediction by metallic spherical droplet model [44]. The size dependent HOMO level (in arbitrary units) of alkali-like metal clusters given by Clemenger-Nilsson ellipsoid shell model [1,45] is also present in Figure 6. In comparison with experiments [7], the present TB calculation has generally reproduced the size dependence of IPs for silver clusters up to 21 atoms but overestimated the IPs of some magic clusters such as Ag_2, Ag_8, and Ag_{18}.

Two characteristic size dependent behaviors are found in Figure 6:

(i) dramatic even-odd alternations where clusters with even number of s valence electrons have higher IPs than their immediate neighbors;
(ii) particular higher IP values at the magic clusters such as Ag_2, Ag_8, Ag_{14}, Ag_{18}, Ag_{20}.

The even-odd variations can be attributed to electron pairing effect. Odd(even)-sized clusters have an odd(even) total number of s valence electrons and the HOMO is singly(doubly) occupied. The electron in a doubly occupied HOMO feels a stronger effective core potential since the electron screening is weaker for the electrons in the same orbital than for inner shell electrons. Therefore, the binding energy of a valence electron in a cluster of even size cluster is larger than that of odd one. It is worthy to note that the size dependence of IPs from TB model is almost in full accordance to Clemenger-Nilsson shell model [45]. The magic effect at Ag_2, Ag_8, Ag_{14}, Ag_{18}, and Ag_{20} predicted by electronic shell model is well reproduced even though the cluster geometries and s–d interaction has been considered. On the other hand, the IP of silver clusters can be roughly described by a classical electrostatic model which take the cluster as a metallic spherical droplet [44]. This fact also suggests that the electronic behavior close to Fermi level of silver clusters are predominantly s-like and the cluster can be roughly approximated to be a jellium sphere with shell-like electronic levels.

5 Conclusion

In conclusion, we have developed a TB model to describe the geometrical and electronic structures of silver clusters. By using GA optimization, the lowest energy structures, binding energies, electronic states, s–d separation, HOMO-LUMO gap, vertical ionization potentials are obtained and compared with experiments. The main results can be summarized in the following points.

(1) The structures of small silver clusters is mostly based on polyhedral packing while planar structure can still exist in very small clusters. The icosahedral growth pattern starts in the Ag_n with $n \geq 11$ and almost dominate the structures of larger clusters.
(2) The electronic shell effect on cluster electronic properties has been found by present TB calculation even through the effect of geometrical structures and d electrons are directly included. The silver clusters with closed electronic shell ($n = 2$, 8, 14, 18, 20) show more pronounced electronic "magic number" characteristics while the geometrical effect is enhanced as the icosahedral shell completes at Ag_{13}.

(3) Due to the pair occupation of s valence electrons on molecular orbitals, silver clusters show even-odd alternation in their relative stability, HOMO-LUMO gap, ionization potential. However, the even-odd effects can be disturbed by the sd overlap and the geometrical effect.
(4) The density of electronic states of smaller silver cluster, *e.g.*, $n < 10$, is composed by discrete sp expanded band and a narrow d band. The bulk-like feature in DOS start at around Ag_{13} and the bulk limit can be roughly reached by $n = 55$.

The present study shows that both the geometrical and electronic effects should be considered in order to achieve a complete description of coinage clusters. Therefore, *ab initio* molecular dynamics or TBMD are essential to elucidate the interplay between geometrical and electronic structures of these clusters. Our further works should include the larger clusters and extend the TB model to other transition metal elements.

This work is partially supported by the U.S. Army Research Office (Grant DAAG55-98-1-0298), NASA Ames Research Center, and the National Natural Science Foundation of China. The authors are deeply grateful to Dr. J. Kohanoff and Dr. J.P. Lu for stimulating discussion and critical reading of manuscript.

References

1. V. Bonačič-Koutecký, P. Fantucci, J. Koutecký, Chem. Rev. **91**, 1035 (1991).
2. W.A. de Heer, Rev. Mod. Phys. **65**, 611 (1993).
3. M. Brack, Rev. Mod. Phys. **65**, 677 (1993).
4. *Clusters of Atoms and Molecules I*, edited by H. Haberland (Springer-Verlag, Berlin, 1995).
5. J.A. Alonso, Chem. Rev. **100**, 637 (2000).
6. I. Katakuse, T. Ichihara, Y. Fujita, T. Matsuo, T. Sakurai, H. Matsuda, Int. J. Mass. Spectrom. In. Proc. **67**, 229 (1985); *ibid.* **74**, 33 (1986).
7. C. Jackschath, I. Rabin, W. Schulze, Z. Phys. D **22**, 517 (1992).
8. G. Alameddin, J. Hunter, D. Cameron, M.M. Kappes, Chem. Phys. Lett. **192**, 122 (1992).
9. J. Ho, K.M. Ervin, W.C. Lineberger, J. Chem. Phys. **93**, 6987 (1990).
10. K.J. Taylor, C.L. Pettiette-Hall, O. Cheshnovsky, R.E. Smalley, J. Chem. Phys. **96**, 3319 (1992).
11. G.F. Ganteför, H. Handschuh, H. Möller, C.Y. Cha, P.S. Bechthold, W. Eberhardt, Surf. Sci. Lett. **3**, 399 (1996); H. Handschuh, C.Y. Cha, P.S. Bechthold, G.F. Ganteför, W. Eberhardt, J. Chem. Phys. **102**, 6406 (1993).
12. J.A. Howard, R. Sutcliffe, B. Mile, Surf. Sci. **156**, 214 (1985) and reference therein.
13. T.L. Hasiett, K.A. Bosnick, M. Moskovits, J. Chem. Phys. **108**, 3453 (1998).
14. J. Tiggesbäumker, L. Köller, K. Meiwes-Broer, A. Liebsch, Phys. Rev. A **48**, 1749 (1993).
15. A. Terasaki, S. Minemoto, M. Iseda, T. Kondow, Eur. Phys. J. D **9**, 163 (1999).
16. A. Hilger, N. Cüppers, M. Tenfeld, U. Kreibig, Eur. Phys. J. D **10**, 115 (2000).
17. D. Reinhard, B.D. Hall, D. Ugarte, R. Monot, Phys. Rev. B **55**, 7868 (1997).
18. U. Hild, G. Dietrich, S. Krückeberg, M. Lindinger, K. Lützenkirchen, L. Schweikhard, C. Walther, J. Ziegler, Phys. Rev. A **57**, 2786 (1998).
19. Y. Shi, V.A. Spasov, K.M. Ervin, J. Chem. Phys. **111**, 938 (1999).
20. C.W. Bauschlicher Jr, S.R. Langhoff, H. Partridge, J. Chem. Phys. **91**, 2412 (1989); J. Chem. Phys. **93**, 8133 (1990); H. Partridge, C.W. Bauschlicher Jr, S.R. Langhoff, Chem. Phys. Lett. **175**, 531 (1990).
21. K. Balasubramanian, M.Z. Liao, Chem. Phys. **127**, 313 (1988); K. Balasubramanian, P.Y. Feng, Chem. Phys. Lett. **159**, 452 (1989); J. Phys. Chem. **94**, 1536 (1990).
22. V. Bonačič-Koutecký, L. Cespiva, P. Fantucci, J. Koutecký, J. Chem. Phys. **98**, 7981 (1993).
23. R. Poteau, J.L. Heully, F. Spiegelmann, Z. Phys. D **40**, 479 (1997).
24. H. Deutsch, J. Pittner, V. Bonačič-Koutecký, K. Becker, S. Matt, T.D. Mark, J. Chem. Phys. **111**, 1964 (1999).
25. R. Car, M. Parrinello, Phys. Rev. Lett. **55**, 2471 (1985).
26. M.C. Payne, M.P. Teter, D.C. Allan, T.A. Arias, J.D. Joannopoulos, Rev. Mod. Phys. **64**, 1045 (1992).
27. C. Massobrio, A. Pasquarello, R. Car, Chem. Phys. Lett. **238**, 215 (1995).
28. Z.F. Lu, W.L. Yim, J.S. Tse, J. Hafner, Eur. Phys. J. D **10**, 105 (2000).
29. C.Z. Wang, K.M. Ho, in *Advances in Chemical Physics*, edited by I. Prigogine, S.A. Rice (John Wiley & Sones, Inc., New York, 1996), Vol. XCIII, p. 651.
30. M. Menon, J. Connolly, N. Lathiotakis, A. Andriotis, Phys. Rev. B **50**, 8903 (1994); N. Lathiotakis, A. Andriotis, M. Menon, J. Connolly, J. Chem. Phys. **104**, 992 (1996).
31. A. Andriotis, N. Lathiotakis, M. Menon, Europhys. Lett. **36**, 37 (1996); Chem. Phys. Lett. **260**, 15 (1996).
32. B. Hartke, Chem. Phys. Lett. **240**, 560 (1995); S.K. Gregurick, M.H. Alexander, B. Hartke, J. Chem. Phys. **104**, 2684 (1996).
33. J.A. Niesse, H.R. Mayne, Chem. Phys. Lett. **261**, 576 (1996); J. Chem. Phys. **105**, 4700 (1996).
34. D.M. Deaven, K.M. Ho, Phys. Rev. Lett. **75**, 288 (1995); D.M. Deaven, N. Tit, J.R. Morris, K.M. Ho, Chem. Phys. Lett. **256**, 195 (1996).
35. Y.H. Luo, J.J. Zhao, S.T. Qiu, G.H. Wang, Phys. Rev. B **59**, 14903 (1999).
36. C. Kittel, *Introduction to Solid State Physics* (John Wiley & Sons, New York, 1986).
37. W.A. Harrison, *Electronic Structure and the Properties of Solids* (Freeman, San Francisco, 1980).
38. D.A. Papaconstantopoulos, *Handbook of the Band Structure of Elemental Solids* (Plenum Press, New York, 1986).
39. M.D. Morse, Chem. Rev. **86**, 1049 (1986).
40. R.A. Perez, L.H. Acevedo, L.A. Thon, J. Chem. Phys. **108**, 5795 (1998).
41. B.J. Winter, E.K. Parks, S.J. Riley, J. Chem. Phys. **94**, 8618 (1991).
42. U. Lammers, G. Borstel, Phys. Rev. B **49**, 17360 (1994).
43. O.B. Christensen, K.W. Jacobsen, J.K. Norskov, M. Manninen, Phys. Rev. Lett. **66**, 2219 (1991).
44. J.P. Perdew, Phys. Rev. B **37**, 6175 (1988).
45. K. Clemenger, Phys. Rev. B **32**, 1359 (1985).
46. A.N. Andriotis, M. Menon, G.E. Froudakis, J.E. Lowther, Chem. Phys. Lett. **301**, 503 (1999).